

Article

Experimental Development of an Innovative Approach to Enhance the Strength of Early Age Cemented Paste Backfill: A Preliminary Investigation of Microwave-Assisted Curing

Mohammed A. Hefni 

Mining Engineering Department, King Abdulaziz University, Jeddah 21589, Saudi Arabia; mhefni@kau.edu.sa; Tel.: +966-599993053

Abstract: In underground mining, the application of mine backfill has evolved into a standard practice. Mine backfill typically consists of tailings, water, and hydraulic binders. However, the high cost of binders has prompted scholars to research alternatives to reduce this cost while maintaining or even improving the properties of the backfill. One potential alternative is leveraging microwave irradiation. In this study, an innovative approach was developed to increase the unconfined compressive strength (UCS) of early age cemented paste backfill (CPB). Microwave treatment was applied to CPB samples at various curing ages for varying durations. The UCS and ultrasonic pulse velocities were measured and analyzed in an experiment with a full factorial design. Moreover, the microstructural properties of the CPB were investigated using mercury intrusion porosimetry. The results indicate a significant potential to increase the UCS of CPB by up to 25% when microwave-treating samples for 8 min after 7 days of curing. This approach could shorten mining cycle times and improve productivity, presenting a promising method to enhance CPB strength.

Keywords: cemented paste backfill; microwave; ultrasonic pulse velocity



Citation: Hefni, M.A. Experimental Development of an Innovative Approach to Enhance the Strength of Early Age Cemented Paste Backfill: A Preliminary Investigation of Microwave-Assisted Curing. *Minerals* **2023**, *13*, 1392. <https://doi.org/10.3390/min13111392>

Academic Editor: Abbas Taheri

Received: 11 September 2023

Revised: 20 October 2023

Accepted: 27 October 2023

Published: 30 October 2023



Copyright: © 2023 by the author. Licensee MDPI, Basel, Switzerland. This article is an open access article distributed under the terms and conditions of the Creative Commons Attribution (CC BY) license (<https://creativecommons.org/licenses/by/4.0/>).

1. Introduction

The expansion of mining operations in recent years has resulted in the increased production of tailings [1], which can represent as much as 99% of the processed ore [2]. Tailings can negatively affect the environment and hinder the sustainable development of the mining industry worldwide [3,4]. Therefore, tailing disposal using a safe and sustainable method is a crucial challenge for the mining industry [5]. One such method is to reuse tailings as a main component in cemented paste backfill (CPB) to backfill cavities created during ore extraction from underground mines. This has become a common practice worldwide to help reduce the environmental impact of tailings and mining costs as deeper mines are excavated and ore production increases [6,7]. CPB contains dewatered tailings (70–85 wt.% solids), binder (traditionally cement), water, and any needed additives [8,9]. A key parameter to consider in CPB design is the development of unconfined compressive strength (UCS) during curing [10]. UCS is affected by the properties of the tailings [11–13], curing method [14], curing time [15], binder type, binder dosage [12,16,17], and the type and amount of additives used [18–21].

Binders account for approximately 75% of the total cost of CPB [22,23]. Increasing the binder content can enhance the mechanical properties of CPB, but it will result in higher costs [24–26]. Further, cement clinker production is associated with high carbon dioxide emissions [27–29]. These considerations have spurred extensive research into alternative binders, such as pozzolanic materials, as partial substitutes for cement. Especially promising from economic and environmental standpoints are industrial wastes with pozzolanic properties [30–32]. Moreover, pozzolanic materials provide resistance to sulfate attack when tailings contain sulfide minerals, which enhances CPB stability and durability [32,33].

A potential method to improve the mechanical properties of CPB without increasing the binder content is to raise the temperature of the CPB during the early stages of curing. The binder hydration rate is positively related to the temperature, and bonding hydration products help to develop CPB strength. A curing temperature of 50 °C appears to be optimal to enhance the UCS, stress–strain behavior, and split tensile strength of CPB [34].

Microwaves have been used for the past 30 years to provide rapid and uniform heating during the curing of cement-based materials like concrete [35–38]. Moreover, it has been reported in the literature that microwave irradiation can be used to assist in underground excavation. For example, Hassani et al. investigated the potential use of microwave-assisted rock breakage in drilling and full-face tunneling machines [39]. Microwave-assisted curing of CPB can similarly be used to reduce mining cycle times and enhance production efficiency, which will ultimately increase a mine’s profitability [34]. Typically, backfill needs to cure for 28 days to gain sufficient strength to serve as a self-standing structure before any adjacent stopes are mined. By accelerating the curing process with microwaving, adjacent stopes could be mined before the 28-day curing period, thus optimizing productivity. The only published study on microwave-assisted curing of CPB showed improved mechanical properties of the CPB samples subjected to microwave radiation [40], but it was limited to curing fresh (<12 h old) CPB samples and with only 7 min of microwave treatment. Further, it did not investigate the effect on CPB pore structure.

Therefore, the novelty of this study is the investigation of how microwave-assisted curing could affect hardened rather than fresh CPB samples. This preliminary bench-scale study was conducted to determine whether the UCS of CPB samples can be improved after 7 days of microwave-assisted curing. A series of laboratory tests and statistically designed experiments were used to assess the main effects of two factors (microwave treatment time and curing age at which CPB samples were microwave-treated) and their interactions with the response variable, UCS, which was both directly measured and estimated using ultrasonic pulse velocity (UPV) tests. The UCS test is widely used to evaluate CPB in laboratories. It is destructive, and significant time is required to prepare samples for testing [41,42], whereas UPV is a rapid, non-destructive means of estimating UCS with a portable and inexpensive system [43–45]. The UPV is strongly correlated ($r = 0.79$) with the UCS of CPB [46]. Finally, selected samples were subjected to mercury intrusion porosimetry (MIP) to understand the effect of microwave-assisted curing on CPB pore size and distribution.

2. Methods

2.1. Materials

Tailings from a gold mine were subjected to sieve analysis for particles coarser than 75 μm , in accordance with ASTM C136-06 [47], and to laser diffraction analysis for particles finer than 75 μm to determine the particle size distribution (Figure 1).

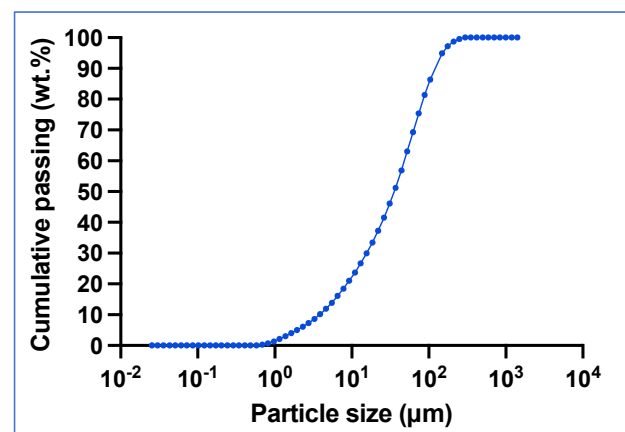


Figure 1. Particle size distribution curve for the tailings.

According to the Unified Soil Classification System, the tailings are well-graded based on their coefficient of uniformity and coefficient of curvature (Table 1). X-ray fluorescence revealed that silicon dioxide (SiO₂) is the principal oxide in the tailings (Table 2). X-ray diffraction analysis, scanning at 2θ from 3° to 80° with a step of 0.02° and a step time of 1 s (Figure 2), indicated that the tailings predominantly comprise anorthite (CaAl₂Si₂O₈), albite (NaAlSi₃O₈), and talc (Mg₃Si₄O₁₀(OH)₂).

Table 1. Physical properties of the studied tailings.

Specific Gravity (g/cm ³)	D ₁₀ ⁽¹⁾ (μm)	D ₃₀ ⁽¹⁾ (μm)	D ₅₀ ⁽¹⁾ (μm)	D ₆₀ ⁽¹⁾ (μm)	D ₉₀ ⁽¹⁾ (μm)	C _u ⁽²⁾	C _c ⁽³⁾	Color
2.80	3.85	17.59	35.82	48.23	120.69	12.53	1.67	Gray

⁽¹⁾ Subscripted numbers indicate the percentage of tailing particles that are finer than each size. ⁽²⁾ Coefficient of uniformity calculated as $\frac{D_{60}}{D_{10}}$. ⁽³⁾ Coefficient of curvature calculated as $\frac{D_{30}^2}{D_{60} \times D_{10}}$.

Table 2. Chemical composition of the studied tailings.

Compound	SiO ₂	Al ₂ O ₃	CaO	MgO	Fe ₂ O ₃	Na ₂ O	C ₂ O ₃	MnO	TiO ₂
Concentration (%)	45.85	19.65	12.70	10.50	5.92	1.18	0.17	0.10	0.10
Compound	K ₂ O	Ni	Zn	V ₂ O ₅	P ₂ O ₅	Co	Cu	Pb	
Concentration (%)	0.09	0.04	0.03	0.01	0.01	<0.01	<0.01	<0.01	

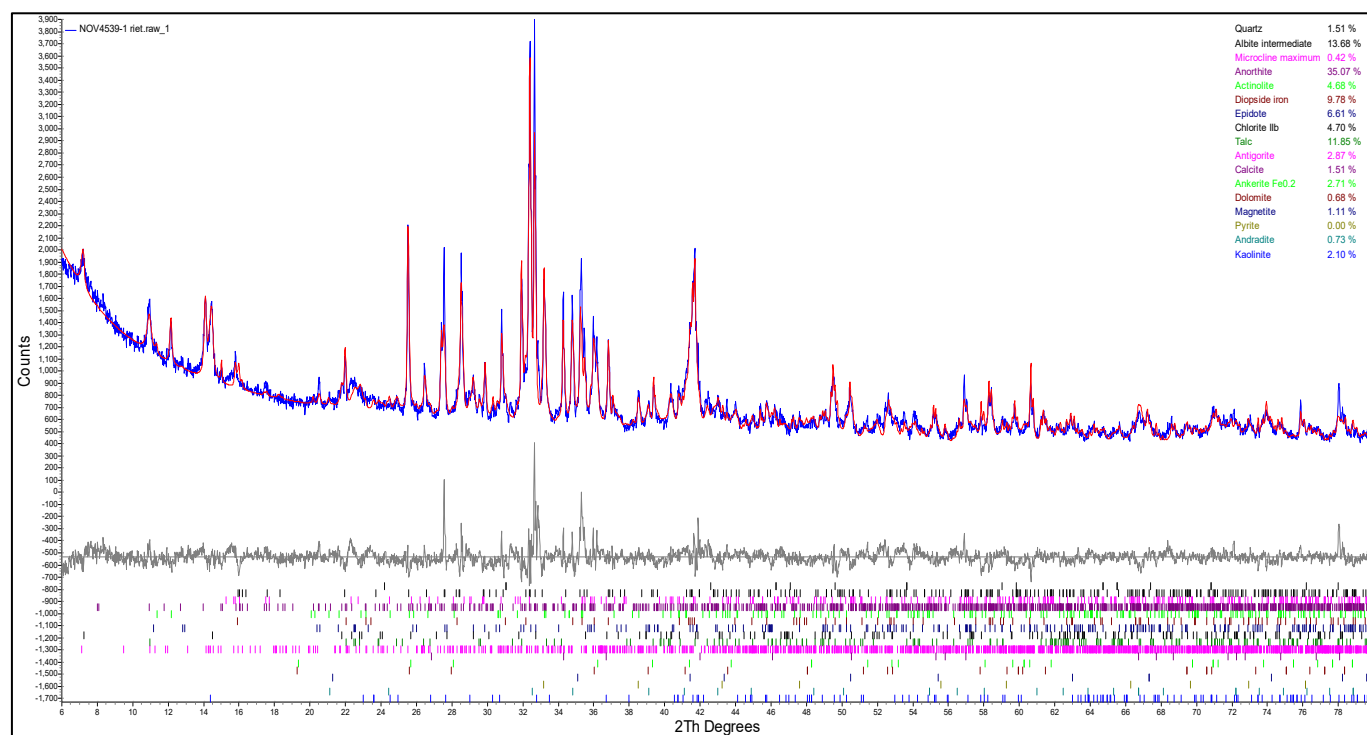


Figure 2. X-ray diffractogram showing mineral phases in the studied tailings.

Table 3 summarizes the elemental composition of the ordinary Portland cement used as the binding agent, as determined using X-ray fluorescence analysis.

Table 3. Chemical composition of the ordinary Portland cement used in this study.

Compound	CaO	SiO ₂	Al ₂ O ₃	MgO	Fe ₂ O ₃	SO ₃	Na ₂ O	K ₂ O	Cl
Concentration (%)	62.53	20.03	4.61	4.28	3.74	2.40	0.20	0.17	0.015

Water from a variety of sources, such as lakes, municipal water supplies, and industrial facilities may be used to prepare mine backfill [34,48]. Cement hydration can be affected by substances in the water. For example, high quantities of dissolved calcium and magnesium aid in the synthesis of hydration products during cement hydration [49]. The properties of the tap water used in this study to prepare the CPB samples are summarized in Table 4.

Table 4. Properties of the mixing water used in this study.

Parameter	pH	Temperature (°C)	Color	Turbidity (NTU)	Total Solids (mg/L)	Conductivity ($\mu\text{S}/\text{cm}$)	Alkalinity (mg/L CaCO_3)	Hardness (mg/L CaCO_3)
Value	7.4	24	colorless	0.16	146	306	93	123

2.2. Sample Preparation and Treatment

The CPB samples were prepared at binder, tailings, and water concentrations of 10, 75.6, and 14.4 wt.%, respectively, in a 5.2 L Cuisinart® stand mixer model SMD-50 series equipped with a digital timer; an inconsistent mixing time can affect CPB properties. After a homogenous paste was obtained, CPB mixtures were poured into microwave-safe 50 mm (inner diameter) \times 100 mm (height) platinum silicon molds supplied by Canadian Silicone Molds. Samples were cured under controlled relative humidity ($90 \pm 2\%$) and temperature ($20 \pm 2^\circ\text{C}$) to mimic underground curing conditions. The schematic diagram in Figure 3 illustrates the preparation steps of the CPB samples and microwave treatment.

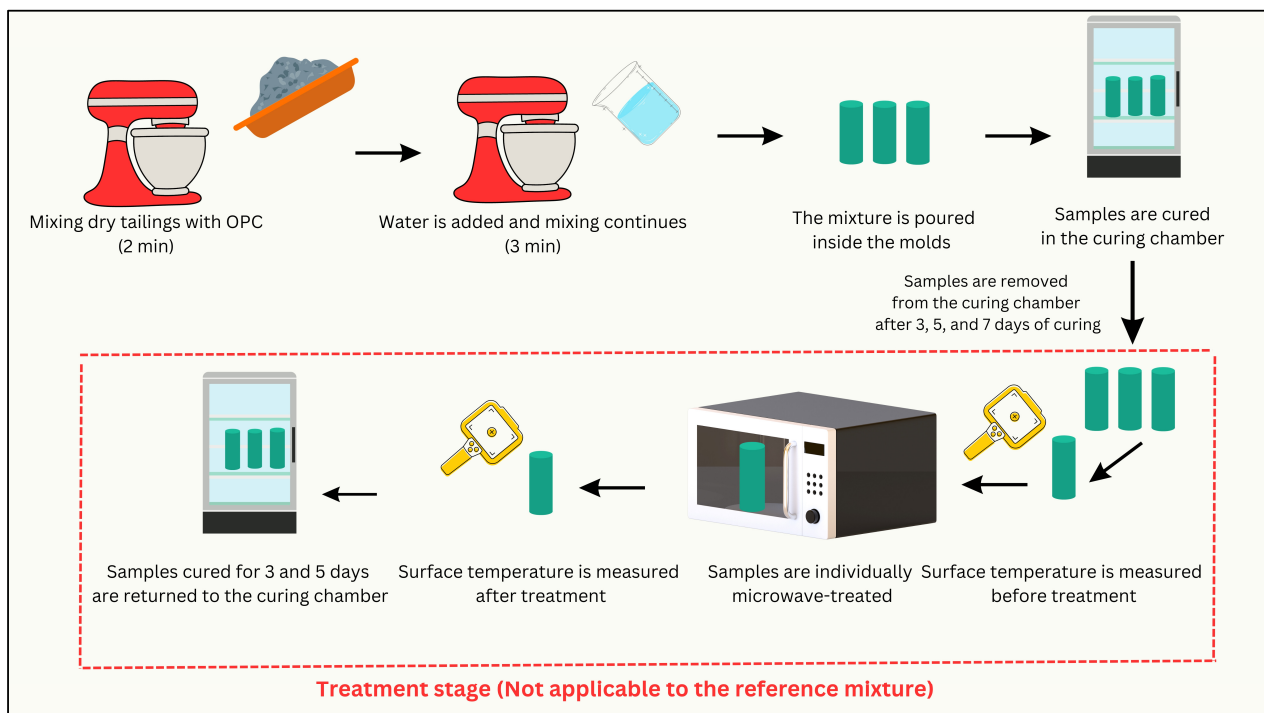


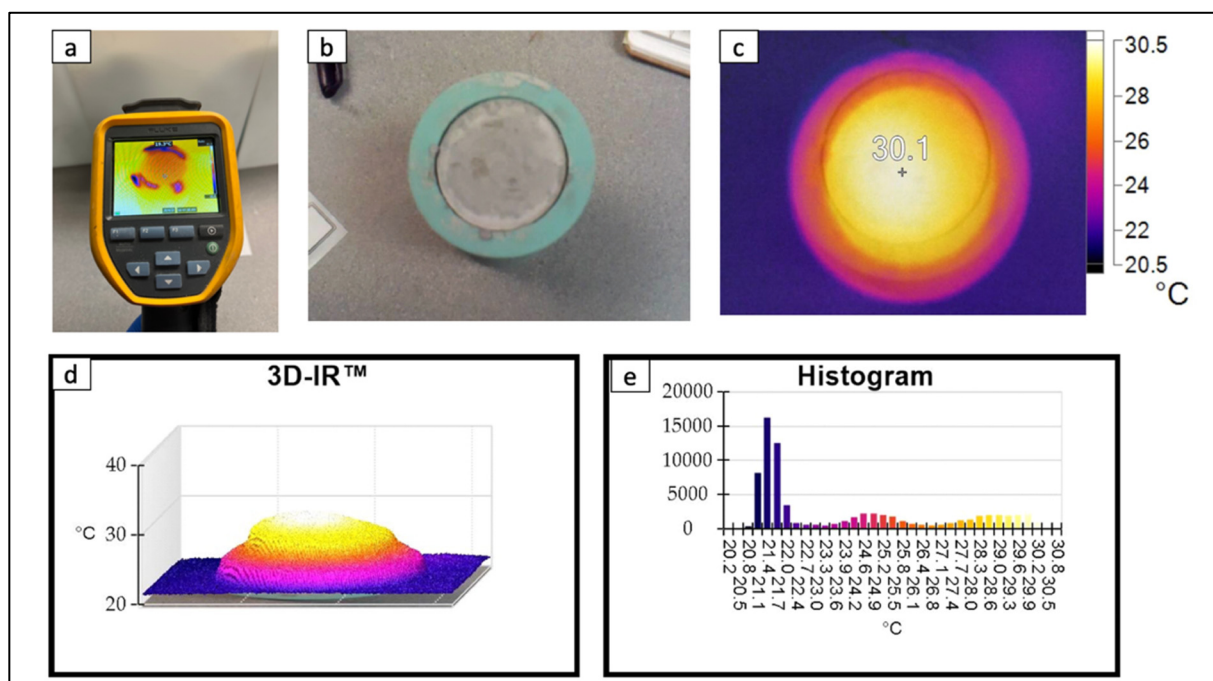
Figure 3. Preparation steps of CPB mixtures and microwave treatment.

The reference samples (no microwave treatment) were not removed from the curing chamber until day 7 (Table 5). The other samples were individually treated for 4, 8, or 12 min in a Toshiba® ML-EM25P(SS) microwave with a capacity of 0.025 m³ and a rated output of 900 W. The lowest power level was used to avoid overheating and to maintain a heating temperature below 50 °C. The samples treated with microwaves at curing days 3 and 5 were returned to the curing chamber until curing day 7. The samples treated with microwaves at curing day 7 were not returned to the curing chamber.

Table 5. Cemented paste backfill treatments and samples tested with mercury intrusion porosimetry (MIP).

Treatment	Microwave Treatment Time (min)	Curing Age (days)	No. Samples Tested with MIP
Reference	0	7	1
1	4	3	-
2	4	5	-
3	4	7	-
4	8	3	-
5	8	5	1
6	8	7	1
7	12	3	-
8	12	5	-
9	12	7	-

Before and after microwave treatment, the surface temperatures of samples were measured with a Fluke® thermal camera model TiS65 (Figure 4a), capable of producing photographs of the sample surfaces (Figure 4b), two- (Figure 4c) and three-dimensional (Figure 4d) temperature profiles, and histograms of the temperature distribution (Figure 4e).

**Figure 4.** (a) Fluke® thermal camera, (b) photograph of a sample's surface, (c) two-dimensional temperature profile, (d) three-dimensional infrared temperature profile, and (e) temperature distribution.

2.3. UCS Tests

Strength tests were conducted on triplicate samples for each treatment in Table 5. Air pressure was used to force the samples out of the molds. Both ends of the samples were carefully trimmed with a grinder (Figure 5a) to ensure the surfaces were level (Figure 5b). A Vernier caliper accurate to 0.01 mm was used to measure sample height and diameter. For UCS tests, a Wykeham Farrance 50 kN loading machine was used in accordance with ASTM D2166 [50]. A 10 kN load cell with a strain control of 1 mm/min compressed each sample until compressive failure (Figure 5c).

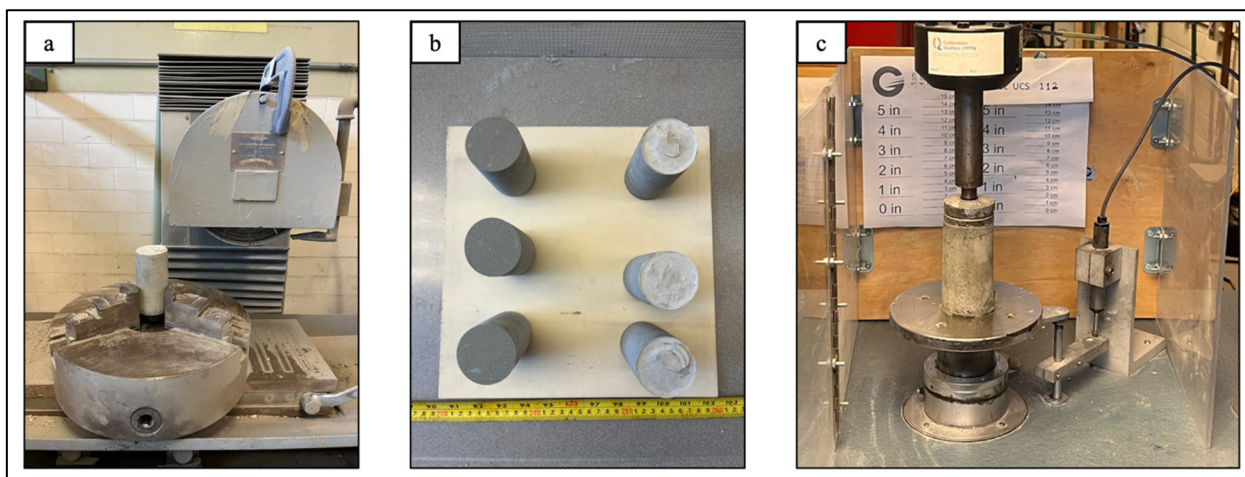


Figure 5. (a) Trimming samples in a grinder. (b) Sample surfaces after (left) and before (right) trimming. (c) Experimental setup for the unconfined compressive strength test.

2.4. UPV Tests

UPV tests were performed on triplicate samples for each treatment in Table 5 and in accordance with ASTM C597-16 [51] using a portable Proceq Pundit Lab[®] instrument (Figure 6), which measures the travel time of a P-wave through a sample between the transmitter and receiver at 54 kHz. Before conducting the test, the transmitter and receiver were coated with an ultrasound gel to make better contact with the samples. A constant pressure of approximately 10 N was applied by hand between the sample surfaces and transducers, following the procedure in [52,53]. This was important to obtain consistent readings. Equation (1) was used to calculate the UPV for each sample.

$$\text{UPV (m/s)} = \left(\frac{\text{length of the samples}}{\text{time measured}} \right) \quad (1)$$



Figure 6. Experimental setup for ultrasonic pulse velocity measurement.

2.5. MIP Tests

MIP tests were used to measure the pore size and pore size distribution in the reference sample and samples 5 and 6 (Table 5). This technique is widely used to assess the pore

structure of cement-based products such as cement pastes, mortars, and concretes [54]. It is suitable for analyzing pores larger than 5 nm [55]. Single samples for each of the three treatments were oven-dried at 100 ± 5 °C. The test was performed by MSE Supplies[®] Analytical Services (Tucson, AZ, USA) using a Micromeritics AutoPore[™] IV 9510 (Figure 7a). A suitable volume of sample (Figure 7b) to fit the penetrometer (Figure 7c) was loaded into the MIP instrument (Figure 7d). Mercury was forced into the samples by increasing the pressure until the sample became saturated. The data were then recorded with the data acquisition system and analyzed in Microsoft Excel.

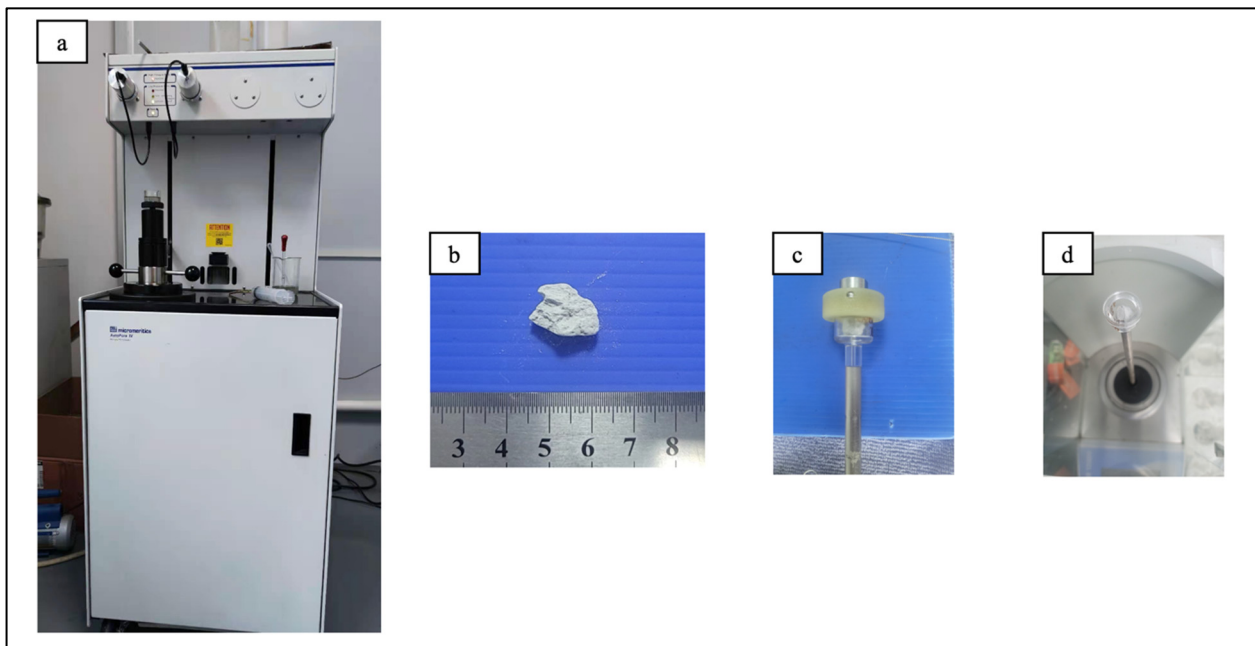


Figure 7. (a) Mercury intrusion porosimeter, (b) cemented paste backfill sample, (c) penetrometer holding the sample, and (d) loading the penetrometer.

2.6. Experimental Design

This study was designed to investigate the effect of microwave treatment time (MT) and the curing age when treated (CA). For each of these two categorical factors, three levels were chosen, for a total of nine runs to produce a full factorial design (Table 5). Alpha was set at 0.05. Two designs were used (Table 6):

1. Design 1 investigated whether UCS and UPV differed between the microwave-treated (measured on curing days 3, 5, and 7) and reference (measured on curing day 7) CPB samples.
2. Design 2 investigated whether increasing the MT at a specific curing age affected CPB strength; it did not consider the reference sample.

Table 6. Factors under investigation for Designs 1 and 2.

Design	Factor	Level 1 (−1)	Level 2 (0)	Level 3 (+1)
1	Microwave treatment time (min)	0	4	8
	Curing age when treated (days)	3	5	7
2	Microwave treatment time (min)	4	8	12
	Curing age when treated (days)	3	5	7

A full factorial design was implemented using JMP Pro 16 to analyze the experimental data. This design entails simultaneously changing numerous factors in a systematic manner

among levels. Analysis of variance (ANOVA) and regression analysis were used to assess differences among the three levels in Table 6 for each factor. Equation (2) expresses a full factorial design with $k = 2$ factors:

$$Y = b_0 + b_1X_1 + b_2X_2 + b_3X_1X_2 + \dots + b_kX_k + \epsilon \tag{2}$$

where Y is the response variable, b_0 is the y-intercept, b_1 and b_2 are coefficients representing the effects of each factor, X_1 to X_k are the coded levels (i.e., -1 for the lowest level, 0 for the medium level, and $+1$ for the highest level), b_3 is the coefficient for the interaction term $X_1 \times X_2$, and ϵ is the error term.

3. Results and Discussion

3.1. Effect of Microwave-Assisted Curing on UCS

The UCS results are shown in Figure 8 and Table 7. The UCS of the reference (untreated) CPB sample was 1.31 MPa after 7 curing days. CPB samples subjected to microwaves on curing days 5 and 7 had the highest UCS (treatments 2, 3, 5, 6, 8, and 9). The maximum UCS, approximately 25% higher than the reference sample, was exhibited by the sample that was microwave-treated for 8 min on curing day 7. Higher UCS values could be attributed to microwaves lowering the water-to-cement ratio, which enhances the interfacial transition zone between the cement paste and aggregates and ultimately leads to higher strength [56]. Research on mortar found that ettringite tends to be shorter after microwave-assisted curing than under normal conditions [56]. A similar mechanism may also apply to CPB.

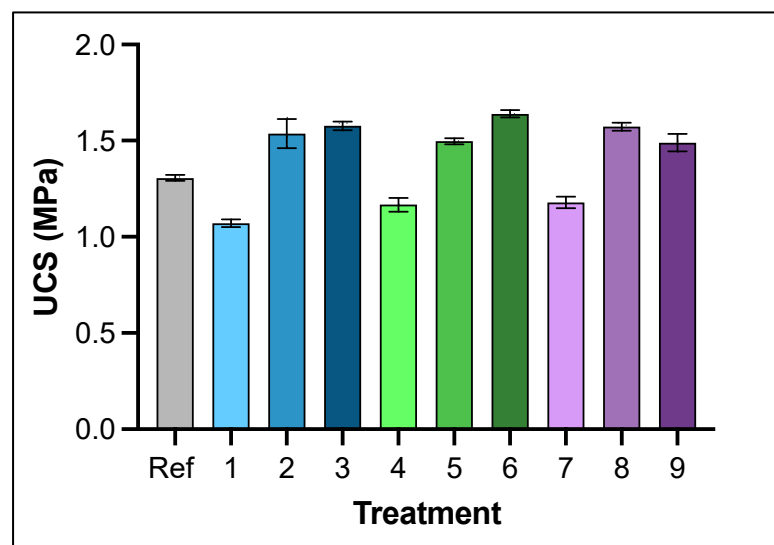


Figure 8. Mean (\pm standard deviation) unconfined compressive strength (UCS) of triplicate cemented paste backfill samples after 7 days of curing for the treatments listed in Table 5.

Table 7. Unconfined compressive strength of triplicate samples for the treatments listed in Table 5.

Treatment	Unconfined Compressive Strength (MPa)				
	Sample 1	Sample 2	Sample 3	Mean	Standard Deviation
Reference	1.29	1.31	1.32	1.31	0.02
1	1.07	1.09	1.05	1.07	0.02
2	1.47	1.52	1.62	1.54	0.08
3	1.55	1.59	1.59	1.58	0.02
4	1.17	1.20	1.13	1.17	0.04
5	1.48	1.50	1.51	1.50	0.02
6	1.64	1.62	1.66	1.64	0.02
7	1.18	1.15	1.21	1.18	0.03
8	1.59	1.55	1.58	1.57	0.02
9	1.53	1.50	1.44	1.49	0.05

Delaying microwave treatment from 3 curing days to 5 and 7 curing days led to an approximately 35% higher mean UCS in the 4- and 8-minute treatment groups (samples 2, 3, 5, and 6 in Figure 8 and Table 7). Microwave treatment at these curing periods may have accelerated cement hydration, promoting the formation of crystals while facilitating the breakdown of amorphous products [57]. On the other hand, among the three samples treated on curing day 7 (samples 3, 6, and 9), the mean UCS was lowest for sample 9, which was treated for 12 min. This could be attributed to a rapid temperature increase that led to water evaporation and air expansion. The expansion stress might have exceeded the tensile strength of the cement paste. A similar pattern was noted by [58], who showed that a 15-minute microwave treatment time resulted in a lower UCS than a 10-minute microwave treatment time for a cement mortar.

The UCS of samples subjected to microwave treatment after 3 curing days (treatments 1, 4, and 7 in Figure 8 and Table 7) were 11%–18% lower than the reference sample. This could be due to a markedly higher temperature achieved on curing day 3 than on curing days 5 and 7 for a given microwave treatment time (Figure 9). Approximately 50% of the heat of hydration is generated after 3 curing days [59] and extra heat is produced by microwave treatment. This could have created a thermal effect that led to the formation of a substantial amount of hydration products coating the cement particles, which impeded further hydration of the cement [57]. Another possibility is that exposure to elevated temperatures led to an uneven distribution of hydration products, which were under development at this stage [60]. This phenomenon, termed the crossover effect, occurs when concrete or cement-based materials are subjected to a higher initial curing temperature, which speeds up hydration but causes uneven distribution of the hydration products.

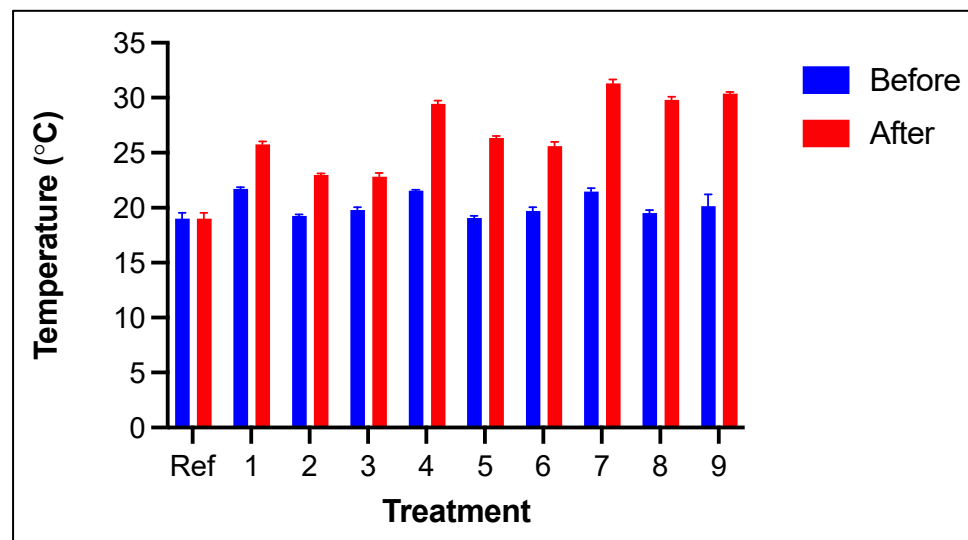


Figure 9. Mean (\pm standard deviation) surface temperatures before and after microwave-assisted curing treatment for the 10 treatments listed in Table 5.

For both Design 1 (Table 8) and Design 2 (Table 9), CA was the main factor influencing UCS. This is due to the quality of hydration products improving at later curing ages, as noted above. The significance of the interaction term in both designs supports the explanation discussed previously (i.e., that both CA and MT affected UCS). MT was expected to be influential in Design 1 since this design incorporated the reference sample: various microwave treatment times altered the UCS compared with the reference sample. However, Design 2 did not include the reference sample, and increasing MT did not result in a significant effect on UCS.

Table 8. Summary of the effects on unconfined compressive strength for Design 1. CA: curing age at which cemented paste backfill samples were microwave-treated; MT: microwave treatment time.







Source	LogWorth		p-Value
CA (days)	13.102		<0.00001
CA (days) × MT (min)	9.734		<0.00001
MT (min)	6.206		<0.00001

Table 9. Summary of the effects on unconfined compressive strength for Design 2. CA: curing age at which cemented paste backfill samples were microwave-treated; MT: microwave treatment time.

Source	LogWorth		p Value
CA (days)	14.600		<0.00001
CA (Days) × MT (min)	3.752		0.00018
MT (min)	1.086		0.08201

The linear regression models for Designs 1 and 2 show excellent agreement between the predicted and measured UCS values ($R^2 = 0.979$ and 0.978 , respectively; Figure 10).

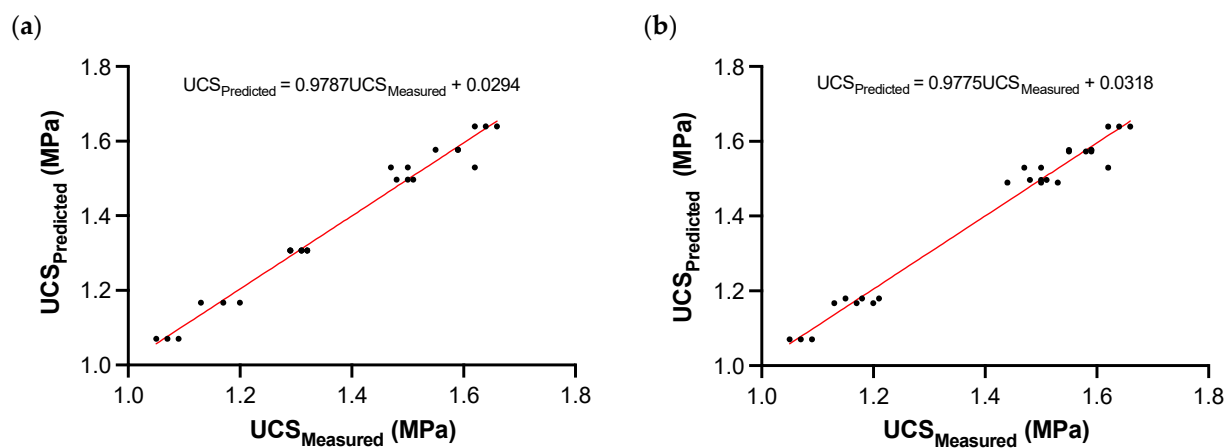


Figure 10. Measured vs. predicted unconfined compressive strength (UCS) for (a) Design 1 and (b) Design 2.

3.2. Effect of Microwave-Assisted Curing on UPV

The UPV results are shown in Figure 11 and Table 10. In contrast to UCS, the UPV for the reference sample was the highest among the treatments. This could be attributed to a higher moisture content: microwave treatment may have enhanced evaporation, leaving behind unoccupied voids, which decrease the UPV by increasing the time required for the wave to travel between the transmitter and receiver [53]. A similar effect was observed in concrete samples from 0 to 100% water saturation [61]. This phenomenon is one reason why UPV is not a perfect metric for UCS.

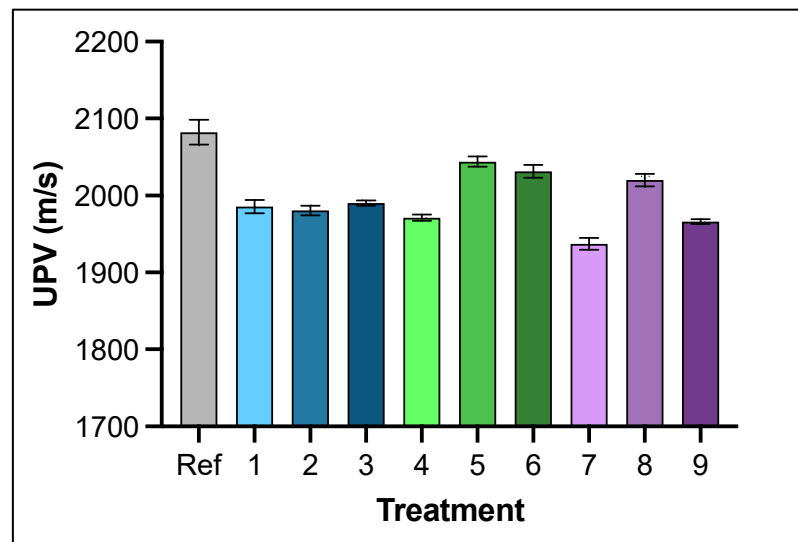


Figure 11. Mean (\pm standard deviation) ultrasonic pulse velocity (UPV) of triplicate cemented paste backfill samples after 7 days of curing for the 10 treatments listed in Table 5.

Table 10. Ultrasonic pulse velocity (UPV) results for the triplicate samples for each treatment group.

Treatment	Ultrasonic Pulse Velocity (m/s)				
	Sample 1	Sample 2	Sample 3	Mean	Standard Deviation
Reference	2065	2085	2097	2082	16.31
1	1985	1977	1994	1985	8.44
2	1975	1988	1979	1981	6.29
3	1987	1990	1994	1990	3.45
4	1971	1967	1975	1971	4.06
5	2051	2042	2038	2044	6.63
6	2023	2031	2040	2031	8.45
7	1945	1929	1937	1937	7.85
8	2011	2025	2025	2020	8.08
9	1965	1963	1969	1966	3.08

Sample 7, which was microwave-treated on curing day 3 for 12 min, had the lowest UPV (Figure 11 and Table 10). As was noted for UCS, this could indicate the formation of inferior-quality hydration products. Among the microwave-treated samples, samples 5 and 6, which were treated on curing days 5 and 7 for 8 min, had the highest UPV. As noted for the UCS results, an improved interfacial transition zone texture may have resulted in denser hydration products. The UPV of the 12-minute treatment tended to be lower when the samples were microwave-treated on curing day 7 (samples 6 and 9) than on curing day 5. Similar to UCS, the expansion stress may have exceeded the tensile strength of the CPB, causing failure of the cement structure.

For both Design 1 (Table 11) and Design 2 (Table 12), CA, MT, and the interaction effect influenced UPV. MT was the main effect in Design 1, while CA was the main effect in Design 2. These results indicate how these factors influenced the internal structure of UCS leading to variation in the UPV values under different microwave curing regimes.

Table 11. Summary of the effects on ultrasonic pulse velocity for Design 1. CA: curing age at which CPB samples were microwave-treated; MT: microwave treatment time.

Source	LogWorth		p-Value
MT (min)	12.078		<0.00001
CA (days) × MT (min)	4.503		0.00003
CA (days)	3.425		0.00038

Table 12. Summary of the effects on ultrasonic pulse velocity for Design 2; CA: curing age at which CPB samples were microwave-treated; MT: microwave treatment time.

Source	LogWorth		p-Value
CA (days)	10.797		<0.00001
MT (min)	9.522		<0.00001
CA (days) × MT (min)	8.592		<0.00001

The linear regression models for Designs 1 and 2 show excellent agreement between the predicted and measured UPV values ($R^2 = 0.962$ and 0.973 , respectively; Figure 12).

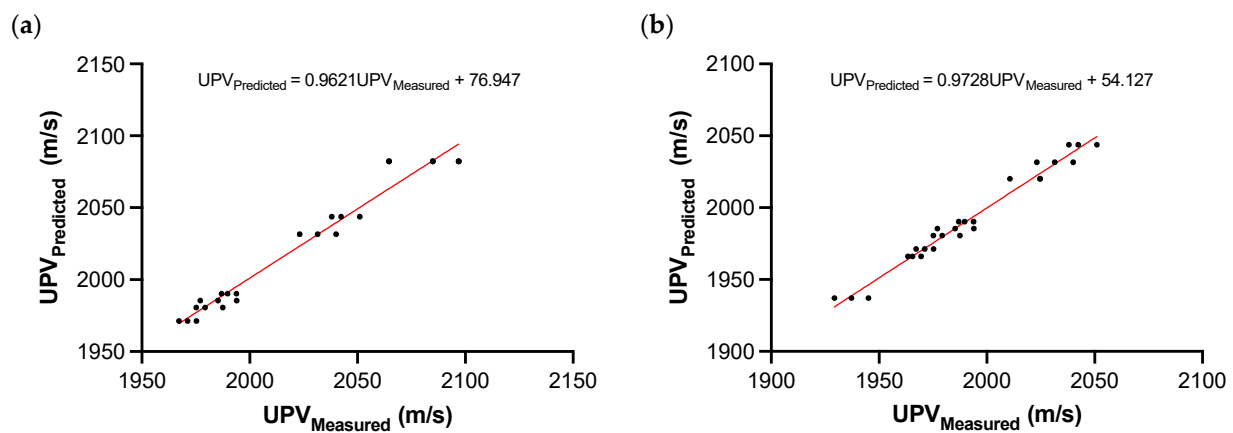


Figure 12. Measured vs. predicted ultrasonic pulse velocity (UPV) for (a) Design 1 and (b) Design 2.

3.3. Effect of Microwave-Assisted Curing on Pore Size Distribution and Porosity

The threshold pore diameter (i.e., the entry pore diameter where mercury begins to enter the interconnected pore network [62]) was approximately 2500 nm for all samples (Figure 13a). The highest total intrusion was in the reference sample (0.3038 mL/g) compared with samples 5 (0.2827 mL/g) and 6 (0.2897 mL/g). These intrusion values equate to porosities of 44.76, 43.20, and 43.58%, respectively. In general, a higher porosity resulted in a lower UCS. The high porosity in the reference sample could be explained by evaporation during oven drying, which created many air-filled voids. Although the three samples had a similar range of pore sizes (approximately 10–2500 nm), the critical (most frequent) pore size [62] was slightly higher for the reference sample (peaks in Figure 13b), which explains why it had the highest porosity. Sample 6 had more small pores than the other two samples, which explains why it had the highest UCS.

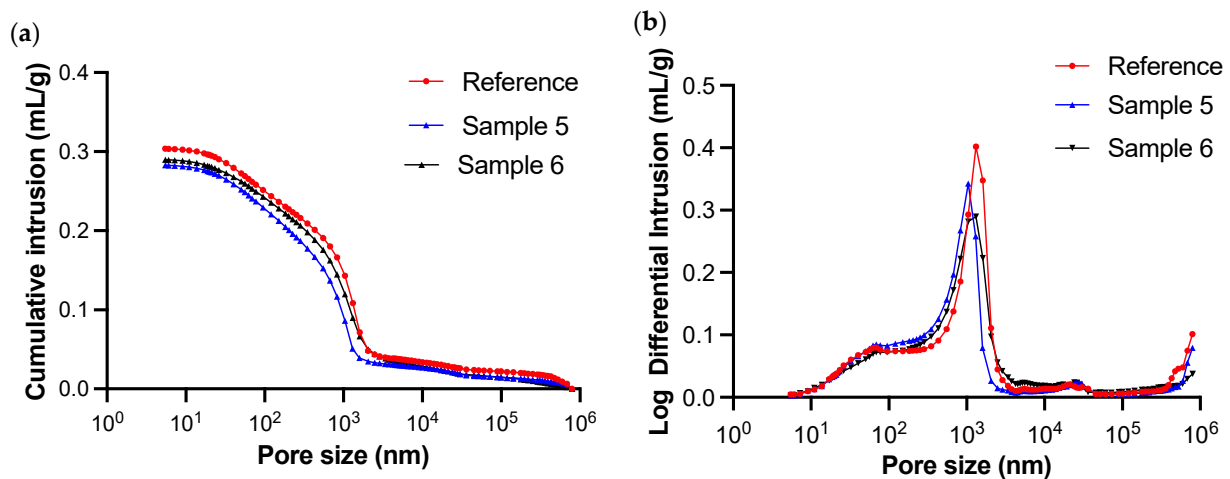


Figure 13. (a) Cumulative intrusion vs. pore size and (b) pore size distribution based on mercury intrusion porosimetry for three cemented paste backfill samples (see Table 4).

4. Conclusions

This preliminary bench-scale investigation tested an innovative approach, microwave-assisted curing, to enhance UCS of the CPB samples. The highest UCS (approximately 35% higher than the reference samples) was achieved using microwave treatment at curing days 5 and 7 when hydration products would have been more developed. This finding is attributed to an enhanced interfacial transition zone and dimensional alterations in ettringite. Microwave treatment after 3 curing days produced the lowest UCS values, possibly because of altered cement hydration and the development of hydration products that prevented further hydration. The longest MT on this curing day, 12 min, resulted in a lower UCS, possibly due to water evaporation and air expansion creating expansion stress that exceeded the CPB tensile strength.

The UCS was also estimated with UPV, which would be a more viable method to measure UCS in situ at a mine site. Overall, the UPV results followed the same trend as the measured UCS results. Small differences were due to the effect of moisture content on the UPV. In contrast to UCS, the reference sample (no microwave treatment) had the highest UPV because microwave treatment drove out moisture, leaving voids or cracks in the CPB that lowered the UPV. The lowest UPV values were observed for CPB samples treated with microwaves for 12 min after 3 curing days. This was attributed to the presence of lower quality hydration products. A better interfacial transition zone texture and denser hydration products in samples treated for 8 min on curing days 5 and 7 led to a higher UPV.

A full factorial design showed that CA, MT, and their interaction effect were significant factors influencing the measured UCS in Design 1, which compared the reference sample to microwave-treated samples. MT was not a significant factor in Design 2, which did not include the reference sample. In Design 1, CA was the main factor influencing the measured UCS, while MT was the main factor influencing the UPV. CA, MT, and their interaction effect were all significant factors for Designs 1 and 2 for UPV results.

MIP testing on the reference and two microwave-treated samples confirmed the mechanisms for some of the observations above. The reference sample had the highest intrusion and porosity, likely due to evaporation of retained moisture during oven drying, resulting in air-occupied voids. The two samples treated for 8 min on curing days 5 and 7 had low intrusion and porosity, but the latter sample had a finer pore structure and correspondingly higher UCS.

This preliminary and experimental investigation is the starting point for field trials to determine the feasibility of this method in real practice. Prototype microwave-assisted drilling machines have been developed for hard rock applications [63]; a similar prototype could be developed for microwave-assisted curing of backfill in stopes.

Funding: This research received no external funding.

Data Availability Statement: All data were included in this paper.

Acknowledgments: The author would like to thank Ferri Hassan, from the Geomechanics Laboratory at McGill University, for technical guidance and research support. Also, the author would like to thank Kirsty Stark and Bill Stark from Canadian Silicone Molds for fabricating the molds used in this study. Finally, the author would like to thank MSE Supplies for performing the MIP test.

Conflicts of Interest: The author declares no conflict of interest.

References

1. Zhao, Y.; Qiu, J.; Wu, P.; Guo, Z.; Zhang, S.; Sun, X. Preparing a binder for cemented paste backfill using low-aluminum slag and hazardous oil shale residue and the heavy metals immobilization effects. *Powder Technol.* **2022**, *399*, 117167. [\[CrossRef\]](#)
2. Lottermoser, B.; Lottermoser, B.G. Tailings. In *Mine Wastes: Characterization, Treatment and Environmental Impacts*; Springer: Berlin/Heidelberg, Germany, 2010; pp. 205–241.
3. Ismail, S.N.; Ramlı, A.; Aziz, H.A. Influencing factors on safety culture in mining industry: A systematic literature review approach. *Resour. Policy* **2021**, *74*, 102250. [\[CrossRef\]](#)
4. Zhao, Y.; Qiu, J.; Guo, Z.; Zhang, S.; Wu, P.; Sun, X. Activation the hydration properties of illite-containing tailings to prepare a binder for cemented paste backfill. *Constr. Build. Mater.* **2022**, *318*, 125989. [\[CrossRef\]](#)
5. Haruna, S.; Fall, M. Reactivity of cemented paste backfill containing polycarboxylate-based superplasticizer. *Miner. Eng.* **2022**, *188*, 107856. [\[CrossRef\]](#)
6. Yang, L.; Yilmaz, E.; Li, J.; Liu, H.; Jiang, H. Effect of superplasticizer type and dosage on fluidity and strength behavior of cemented tailings backfill with different solid contents. *Constr. Build. Mater.* **2018**, *187*, 290–298. [\[CrossRef\]](#)
7. Qi, C.; Fourie, A.; Chen, Q. Neural network and particle swarm optimization for predicting the unconfined compressive strength of cemented paste backfill. *Constr. Build. Mater.* **2018**, *159*, 473–478. [\[CrossRef\]](#)
8. Fall, M.; Benzaazoua, M.; Saa, E. Mix proportioning of underground cemented tailings backfill. *Tunn. Undergr. Space Technol.* **2008**, *23*, 80–90. [\[CrossRef\]](#)
9. Orejarena, L.; Fall, M. Mechanical response of a mine composite material to extreme heat. *Bull. Eng. Geol. Environ.* **2008**, *67*, 387–396. [\[CrossRef\]](#)
10. Niu, H.; Hassani, F.P.; Kermani, M.F.; He, M. Rheological and mechanical properties of fibre-reinforced cemented paste and foam backfill. *Int. J. Min. Reclam. Environ.* **2021**, *35*, 488–505. [\[CrossRef\]](#)
11. Fall, M.; Benzaazoua, M.; Ouellet, S. Experimental characterization of the influence of tailings fineness and density on the quality of cemented paste backfill. *Miner. Eng.* **2005**, *18*, 41–44. [\[CrossRef\]](#)
12. Kesimal, A.; Yilmaz, E.; Ercikdi, B. Evaluation of paste backfill mixtures consisting of sulphide-rich mill tailings and varying cement contents. *Cem. Concr. Res.* **2004**, *34*, 1817–1822. [\[CrossRef\]](#)
13. Kesimal, A.; Yilmaz, E.; Ercikdi, B.; Alp, I.; Deveci, H. Effect of properties of tailings and binder on the short-and long-term strength and stability of cemented paste backfill. *Mater. Lett.* **2005**, *59*, 3703–3709. [\[CrossRef\]](#)
14. De Araújo, E.E.B.; Simon, D.; de França, F.A.N.; de Freitas Neto, O.; dos Santos, O.F., Jr. Shear strength of a cemented paste backfill submitted to high confining pressure. *Appl. Mech. Mater.* **2017**, *858*, 219–224. [\[CrossRef\]](#)
15. Yilmaz, E.; Belem, T.; Bussi ere, B.; Mbonimpa, M.; Benzaazoua, M. Curing time effect on consolidation behaviour of cemented paste backfill containing different cement types and contents. *Constr. Build. Mater.* **2015**, *75*, 99–111. [\[CrossRef\]](#)
16. Ercikdi, B.; Yilmaz, T.; K ulekci, G. Strength and ultrasonic properties of cemented paste backfill. *Ultrasonics* **2014**, *54*, 195–204. [\[CrossRef\]](#)
17. Ercikdi, B.; Kesimal, A.; Cihangir, F.; Deveci, H.; Alp, İ. Cemented paste backfill of sulphide-rich tailings: Importance of binder type and dosage. *Cem. Concr. Compos.* **2009**, *31*, 268–274. [\[CrossRef\]](#)
18. Mitchell, R.J.; Stone, D.M. Stability of reinforced cemented backfills. *Can. Geotech. J.* **1987**, *24*, 189–197. [\[CrossRef\]](#)
19. Kermani, M.; Hassani, F.; Aflaki, E.; Benzaazoua, M.; Nokken, M. Evaluation of the effect of sodium silicate addition to mine backfill, Gelfill—Part 1. *J. Rock Mech. Geotech. Eng.* **2015**, *7*, 266–272. [\[CrossRef\]](#)
20. Koohestani, B.; Belem, T.; Koubaa, A.; Bussi ere, B. Experimental investigation into the compressive strength development of cemented paste backfill containing Nano-silica. *Cem. Concr. Compos.* **2016**, *72*, 180–189. [\[CrossRef\]](#)
21. Mangane, M.B.C.; Argane, R.; Trauchessec, R.; Lecomte, A.; Benzaazoua, M. Influence of superplasticizers on mechanical properties and workability of cemented paste backfill. *Miner. Eng.* **2018**, *116*, 3–14. [\[CrossRef\]](#)
22. Grice, T. Underground mining with backfill. In *Proceedings of the 2nd Annual Summit   Mine Tailings Disposal Systems*, Brisbane, QLD, Australia, 24 November 1998; pp. 24–25.
23. Jiang, H.; Ren, L.; Zhang, Q.; Zheng, J.; Cui, L. Strength and microstructural evolution of alkali-activated slag-based cemented paste backfill: Coupled effects of activator composition and temperature. *Powder Technol.* **2022**, *401*, 117322. [\[CrossRef\]](#)
24. Potvin, Y.; Thomas, E.; Fourie, A. *Handbook on Mine Fill*; Australian Centre for Geomechanics: Crawley, Australia, 2005; p. 179.
25. Li, H.; Wu, A.; Wang, H. Evaluation of short-term strength development of cemented backfill with varying sulphide contents and the use of additives. *J. Environ. Manag.* **2019**, *239*, 279–286. [\[CrossRef\]](#) [\[PubMed\]](#)

26. Yilmaz, E.; Yilmaz, E. Sustainability and tailings management in the mining industry: Paste technology. *Mugla J. Sci. Technol.* **2018**, *4*, 16–26. [[CrossRef](#)]
27. Srividhya, S.; Vidjeapriya, R.; Neelamegam, M. Enhancing the performance of hyposludge concrete beams using basalt fiber and latex under cyclic loading. *Comput. Concr.* **2021**, *28*, 93.
28. Prakash, R.; Thenmozhi, R.; Raman, S. Mechanical characterisation and flexural performance of eco-friendly concrete produced with fly ash as cement replacement and coconut shell coarse aggregate. *Int. J. Environ. Sustain. Dev.* **2019**, *18*, 131–148. [[CrossRef](#)]
29. Prakash, R.; Raman, S.N.; Subramanian, C.; Divyah, N. Eco-friendly fiber-reinforced concretes. In *Handbook of Sustainable Concrete and Industrial Waste Management*; Elsevier: Amsterdam, The Netherlands, 2022; pp. 109–145.
30. Peyronnard, O.; Benzaazoua, M. Alternative by-product based binders for cemented mine backfill: Recipes optimisation using Taguchi method. *Miner. Eng.* **2012**, *29*, 28–38. [[CrossRef](#)]
31. Ercikdi, B.; Cihangir, F.; Kesimal, A.; Deveci, H.; Alp, İ. Utilization of industrial waste products as pozzolanic material in cemented paste backfill of high sulphide mill tailings. *J. Hazard. Mater.* **2009**, *168*, 848–856. [[CrossRef](#)]
32. Niroshan, N.; Sivakugan, N.; Veenstra, R.L. Laboratory study on strength development in cemented paste backfills. *J. Mater. Civ. Eng.* **2017**, *29*, 04017027. [[CrossRef](#)]
33. Sivakugan, N.; Rankine, R.; Rankine, K.; Rankine, K. Geotechnical considerations in mine backfilling in Australia. *J. Clean. Prod.* **2006**, *14*, 1168–1175. [[CrossRef](#)]
34. Fall, M.; Célestin, J.; Pokharel, M.; Touré, M. A contribution to understanding the effects of curing temperature on the mechanical properties of mine cemented tailings backfill. *Eng. Geol.* **2010**, *114*, 397–413. [[CrossRef](#)]
35. Graytee, A.; Sanjayan, J.G.; Nazari, A. Development of a high strength fly ash-based geopolymer in short time by using microwave curing. *Ceram. Int.* **2018**, *44*, 8216–8222. [[CrossRef](#)]
36. Chindapasirt, P.; Rattanasak, U.; Taebuanhuad, S. Role of microwave radiation in curing the fly ash geopolymer. *Adv. Powder Technol.* **2013**, *24*, 703–707. [[CrossRef](#)]
37. Tanaka, H.; Fujii, A.; Fujimoto, S.; Tanaka, Y. Microwave-assisted two-step process for the synthesis of a single-phase Na-A zeolite from coal fly ash. *Adv. Powder Technol.* **2008**, *19*, 83–94. [[CrossRef](#)]
38. Hutchison, R.; Chang, J.; Jennings, H.M.; Brodwin, M. Thermal acceleration of Portland cement mortars with microwave energy. *Cem. Concr. Res.* **1991**, *21*, 795–799. [[CrossRef](#)]
39. Hassani, F.; Nekoovaght, P.M.; Gharib, N. The influence of microwave irradiation on rocks for microwave-assisted underground excavation. *J. Rock Mech. Geotech. Eng.* **2016**, *8*, 1–15. [[CrossRef](#)]
40. Wu, D.; Sun, W.; Liu, S.; Qu, C. Effect of microwave heating on thermo-mechanical behavior of cemented tailings backfill. *Constr. Build. Mater.* **2021**, *266*, 121180. [[CrossRef](#)]
41. Liu, L.; Miramini, S.; Hajimohammadi, A. Characterising fundamental properties of foam concrete with a non-destructive technique. *Nondestruct. Test. Eval.* **2019**, *34*, 54–69. [[CrossRef](#)]
42. Xu, W.; Tian, X.; Wan, C. *Prediction of Mechanical Performance of Cemented Paste Backfill by the Electrical Resistivity Measurement*; ASTM International: West Conshohocken, PA, USA, 2018.
43. Xu, S.; Suorineni, F.T.; Li, K.; Li, Y. Evaluation of the strength and ultrasonic properties of foam-cemented paste backfill. *Int. J. Min. Reclam. Environ.* **2017**, *31*, 544–557. [[CrossRef](#)]
44. Simon, D.; Grabinsky, M.W. Electromagnetic wave-based measurement techniques to study the role of Portland cement hydration in cemented paste backfill materials. *Int. J. Min. Reclam. Environ.* **2012**, *26*, 3–28. [[CrossRef](#)]
45. Xu, W.; Tian, X.; Cao, P. Assessment of hydration process and mechanical properties of cemented paste backfill by electrical resistivity measurement. *Nondestruct. Test. Eval.* **2018**, *33*, 198–212. [[CrossRef](#)]
46. Yilmaz, T.; Ercikdi, B. Predicting the uniaxial compressive strength of cemented paste backfill from ultrasonic pulse velocity test. *Nondestruct. Test. Eval.* **2016**, *31*, 247–266. [[CrossRef](#)]
47. ASTM C136-06; Standard Test Method for Sieve Analysis of Fine and Coarse Aggregates. ASTM International: West Conshohocken, PA, USA, 2006.
48. Jiang, H.; Qi, Z.; Yilmaz, E.; Han, J.; Qiu, J.; Dong, C. Effectiveness of alkali-activated slag as alternative binder on workability and early age compressive strength of cemented paste backfills. *Constr. Build. Mater.* **2019**, *218*, 689–700. [[CrossRef](#)]
49. Wu, A.; Wang, Y.; Wang, H.; Yin, S.; Miao, X. Coupled effects of cement type and water quality on the properties of cemented paste backfill. *Int. J. Miner. Process.* **2015**, *143*, 65–71. [[CrossRef](#)]
50. ASTM. D2166; Standard Test Method for Unconfined Compressive Strength of Cohesive Soil. ASTM International: West Conshohocken, PA, USA, 2016.
51. ASTM. C597; Standard Test Method for Pulse Velocity through Concrete. ASTM International: West Conshohocken, PA, USA, 2016.
52. Jiang, H.; Han, J.; Li, Y.; Yilmaz, E.; Sun, Q.; Liu, J. Relationship between ultrasonic pulse velocity and uniaxial compressive strength for cemented paste backfill with alkali-activated slag. *Nondestruct. Test. Eval.* **2020**, *35*, 359–377. [[CrossRef](#)]
53. Sari, M.; Yilmaz, E.; Kasap, T.; Karasu, S. Exploring the link between ultrasonic and strength behavior of cementitious mine backfill by considering pore structure. *Constr. Build. Mater.* **2023**, *370*, 130588. [[CrossRef](#)]
54. Ma, H. Mercury intrusion porosimetry in concrete technology: Tips in measurement, pore structure parameter acquisition and application. *J. Porous Mater.* **2014**, *21*, 207–215. [[CrossRef](#)]

55. Aligizaki, K.K. *Pore Structure of Cement-Based Materials: Testing, Interpretation and Requirements*; Crc Press: Boca Raton, FL, USA, 2005.
56. Kong, Y.; Wang, P.; Liu, S.; Gao, Z. Hydration and microstructure of cement-based materials under microwave curing. *Constr. Build. Mater.* **2016**, *114*, 831–838. [[CrossRef](#)]
57. Gao, Z.; He, Y.; Li, M.; Jiang, M.; Shen, J. Impacts of microwave on hydration evolution of Portland cement in the perspective of composition and microstructure of hydrates. *Constr. Build. Mater.* **2022**, *360*, 129569. [[CrossRef](#)]
58. Yan, G.; Li, J.; Lin, Y.; Chen, X. Difference between Internal and External Hydration of Hardened Cement Paste under Microwave Curing. *Adv. Mater. Sci. Eng.* **2021**, *2021*, 3307325. [[CrossRef](#)]
59. De Rojas Gómez, M.S.; Rojas, M.F. Natural pozzolans in eco-efficient concrete. In *Eco-Efficient Concrete*; Elsevier: Amsterdam, The Netherlands, 2013; pp. 83–104.
60. Yousuf, S.; Shafiqh, P.; Ibrahim, Z.; Hashim, H.; Panjehpour, M. Crossover effect in cement-based materials: A review. *Appl. Sci.* **2019**, *9*, 2776. [[CrossRef](#)]
61. Candelaria, M.D.E.; Kee, S.-H.; Yee, J.-J.; Lee, J.-W. Effects of saturation levels on the ultrasonic pulse velocities and mechanical properties of concrete. *Materials* **2020**, *14*, 152. [[CrossRef](#)] [[PubMed](#)]
62. Hewlett, P.; Liska, M. *Lea's Chemistry of Cement and Concrete*, 4th ed.; Butterworth-Heinemann: Oxford, UK, 2019.
63. Hassani, F.; Nekoovaght, P. The development of microwave assisted machineries to break hard rocks. In Proceedings of the 28th International Symposium on Automation and Robotics in Construction (ISARC), Seoul, Republic of Korea, 29 June–2 July 2011; pp. 678–684.

Disclaimer/Publisher's Note: The statements, opinions and data contained in all publications are solely those of the individual author(s) and contributor(s) and not of MDPI and/or the editor(s). MDPI and/or the editor(s) disclaim responsibility for any injury to people or property resulting from any ideas, methods, instructions or products referred to in the content.